J. Fluid Mech. (1984), *vol.* 142, *pp.* 121–149
Printed in Great Britain

Study of turbulent structure with hot wires smaller than the viscous length

By WILLIAM W. WILLMARTH AND LALIT K. SHARMA†
Department of Aerospace Engineering, University of Michigan, Ann Arbor, Michigan 48109

(Received 18 September 1980 and in revised form 4 January 1984)

The small-scale structure of the streamwise velocity fluctuations in the wall region of a turbulent boundary layer is examined in a new wind-tunnel facility using hot-wires smaller than any previously constructed (typical dimensions: $l = 25$ μm, $d = 0.5$ μm). In the boundary layer in which the measurements were made, the ratio of the hot-wire length to the viscous length is 0.3. The turbulent intensity measured with the small hot wires is larger than that measured with longer wires owing to the better spatial resolution of the small wires. The velocity fluctuations measured by the small hot wires are also analysed to determine the burst frequency at two Reynolds numbers and at various distances from the wall. The dimensionless burst frequency does not depend on the Reynolds number when scaled with wall parameters. However, it increases with Reynolds number when scaled with outer variables. Velocity fluctuations measured by two hot wires, less than two viscous lengths apart, are analysed to reveal the small-scale features present during a burst and in the absence of a burst. The main conclusions are: (1) intermittent small-scale shear layers occur most frequently when bursts are present, less frequently just after a burst, and even less frequently just before a burst; and (2) on occasion the velocity gradient of the small-scale shear layers is as large as the mean-velocity gradient at the wall.

1. Introduction

In the wall region of the turbulent boundary layer the root-mean-square turbulent velocity fluctuations are large; a maximum root-mean-square velocity of 30% of the local mean velocity is found at a distance of 13 viscous lengths‡ from the wall. Measurements with hot-wire probes have shown that the turbulent-energy production, Reynolds stress and viscous dissipation are also a maximum at this distance from the wall. Using flow-visualization methods, Corino & Brodkey (1969) and Kim, Kline & Reynolds (1971) have studied the phenomenon of bursting in which energetic turbulent motions occur in the region near the wall. Their investigations, and many others since that time, have shown that the bulk of the contributions to turbulent energy production and Reynolds stress occur during bursting.

As explained in detail below, recent investigations of turbulence in the region near the wall have shown that at high Reynolds numbers the scale of turbulence is very small. The present study was designed to provide new measurements at high Reynolds numbers, using the smallest hot wires that we could fabricate, in an attempt to obtain more information about the small-scale structure of turbulence.

The existence of small-scale turbulent structure in the wall region was first observed in a visual study. Fage & Townend (1932) employed an ultramicroscope to

† Present address: Rockwell Intl Rocketdyne Div., Canoga Park, California.

‡ The viscous length is ν/u_τ, where $u_\tau = (\tau_w/\rho)^{\frac{1}{2}}$ is the friction velocity.

examine fluid motion very near the wall for turbulent flow in a square tube. In the region $0 < y^+ < 4$† they observed continual departures of the motion of fluid elements from truly rectilinear flow. They measured the angle between the tube axis and the direction of motion of particles suspended in the fluid at various distances from the wall. They found a maximum angle of 27° in a plane parallel to the wall and a maximum angle of 10° in a plane parallel to the stream and normal to the wall.

Corino & Brodkey (1969) used a high-speed ciné camera to photograph the trajectories of very small particles suspended in a fully turbulent flow of trichloroethylene in a pipe. In their photographs of a thin illuminated plane of fluid, oriented parallel to the stream and normal to the wall, a two-layer phenomenon was occasionally observed in which the particles appeared to be moving in different directions at the same point. The photographs had a depth of field of the order of 20 viscous lengths. The two-layer phenomena was often observed during bursting (a burst being defined as low-speed fluid moving away from the wall) which was direct evidence that substantial velocity variations within a distance of less than 20 viscous lengths were common during bursting.

Kim *et al.* (1971) used a combined dye-injection and hydrogen-bubble technique to perform visual observations and quantitative measurements in the turbulent boundary layer in a water channel. They observed a series of low-speed streaks having a more or less regular spanwise spacing in the region $0 < y^+ < 10$. The streaks were a part of the phenomenon that Kline *et al.* (1967) called 'bursting' – a sequence of events related to the production of turbulence. Their quantitative data showed that the bursting process could be described as made up of three stages:

(i) lifting of the low-speed streaks from the innermost layer;

(ii) growth of an oscillatory motion which remains quite 'organized' for 3–10 cycles; and

(iii) breakup of the oscillatory, well-defined motion into more random or chaotic motions, accompanied by a return to the wall of a low-speed streak, and a more-quiescent flow.

Kim *et al.* estimated that the bursting process is responsible for all the turbulent production in the region $0 < y^+ < 90$. Corino & Brodkey, in their visual study, estimated that 70% of the turbulent production took place during the bursting process in the same region. Using hot-wire anemometers in an X-array, Lu & Willmarth (1972) reported that 'throughout the turbulent boundary layer, the bursts are the largest contributors to the Reynolds stress $\overline{uv}$, with sweeps the second largest'. Lu & Willmarth's studies showed that, on the average, the burst events account for 77% of the contributions to Reynolds stress. Thus, the bursting process is an important feature of the structure of turbulence near the wall.

Kim *et al.* often observed small-scale streamwise vortices during bursting. Based on this observation and on their own data, Willmarth & Bogar (1977) suggested that the streamwise vortical flow structure is primarily responsible for intense small-scale velocity gradients in the turbulent flow near the wall.

Further evidence that the turbulent structure near the wall is of a very small scale has also been provided by Emmerling (1973). Using an optical method to measure the deflection of a membrane covering an array of small-diameter holes in the wall, Emmerling observed small-scale convected pressure fluctuations which were on occasion of smaller scale than the diameter (55 viscous lengths) of the membrane-covered holes. Emmerling also measured the root-mean-square wall-pressure fluctu-

† The superscript + denotes a dimensionless quantity scaled with wall parameters, i.e. $y^+ = y/(\nu/u_\tau)$.

ations using pinhole microphones of various diameters. His measurements of the intensity of the pressure fluctuations as a function of pinhole diameter d were constant for $d^+ > 100$, but for $d^+ < 100$ the intensity began to rise dramatically. At $d^+ = 18$ the intensity was more than doubled, and the trend was toward larger values at even smaller diameters. However, Bull & Thomas (1976) also made measurements of the wall-pressure fluctuations using very small transducers flush with the surface. Their measurements confirmed the existence of small-scale pressure fluctuations but showed that the measurements with pinhole microphones overestimated the intensity of the fluctuations, owing to aerodynamic interaction of the flow within the pinhole and the boundary-layer flow. The actual root-mean-square pressure fluctuations for transducer diameters of the order of 20 viscous lengths were 50 % larger than the value measured for transducers 100 viscous lengths in diameter. This result indicates that wall-pressure fluctuations with scales less than 100 viscous lengths are of comparable intensity to those with scales greater than 100 viscous lengths.

A detailed investigation of the structure of turbulence in the wall region of a fully turbulent channel flow, beginning with the work of Eckelmann (1974), is continuing (see e.g. Kreplin & Eckelmann 1979). In their work, Eckelmann and his colleagues have been using an oil channel to produce a wall-bounded flow with a very large viscous length. In this flow, conventionally sized hot-film probes are used since the probe dimensions are of the order of only two viscous lengths. The measurements of Eckelmann and his colleagues are unique because they have been able to obtain detailed measurements, as a function of time, of turbulent-velocity components, Reynolds stress, dissipation and numerous other quantities well within the viscous layer a few viscous lengths from the wall. However, their measurements in the oil channel were made at low flow speeds in order that the viscous length would be large, which means that the Reynolds number of their flow is also quite low. Their Reynolds number was approximately 4000, based on the centreline velocity and the half-width of the channel. This value is very much less than the Reynolds number at which most of the conventional investigations of the turbulence in boundary layers have been made. The typical Reynolds number of investigations in wind tunnels ranges from 10000 to 1000000, based on freestream velocity and boundary-layer thickness.

For investigations in wind tunnels at high Reynolds numbers, the relative size of the conventional hot wires is much greater than the viscous length. Willmarth & Bogar (1977) recognized this, and developed a small hot-wire probe in an attempt to resolve the small-scale structure of turbulence. The probe they constructed was an extremely small X-array of two hot wires with a typical length and spacing of 100 μm. Measurements were made using this probe in a wind-tunnel boundary layer at a Reynolds number of 117000 (based on freestream velocity and boundary-layer thickness). In this boundary layer, the characteristic dimensions of the X-array were 2.5 viscous lengths. When measurements near the wall were attempted there were numerous occasions when erroneous measurements of the turbulent velocity fluctuations were made by the array. Specifically, the erroneous signals from the X-array were pairs of output voltages that were not observed during calibration of the X-array in a uniform flow. At a distance of 10 viscous lengths from the wall, the erroneous signals occurred 19 % of the time. The erroneous measurements were attributed to the inability of the X-hot-wire array to resolve the small-scale turbulence accurately near the wall. The fact that the hot-wire measurements were in error was cited as evidence of the existence of very-small-scale turbulence in the boundary layer near the wall.

From the results of the previous investigations described above, we believe that

at high Reynolds numbers very-small-scale turbulence exists in the boundary layer near the wall. If this is the case, measurements in turbulent boundary layers made with conventionally sized probes, at high Reynolds numbers, suffer from the poor spatial resolution of small-scale phenomena that are present, especially near the wall. The present investigation was designed to investigate further the smallest scales of turbulence in boundary layers at high Reynolds numbers. A new wind tunnel was constructed for this investigation which produces a high-Reynolds-number boundary layer with a large viscous length. The investigation was made using hot wires smaller than the viscous length.

2. Experimental apparatus and methods

2.1. *Wind tunnel*

A new wind tunnel was designed for this investigation which produces a fully developed turbulent boundary layer at high Reynolds number with a large viscous length. A large viscous length can be obtained by increasing the kinematic viscosity (by heating the air or by the use of fluids other than air) and/or by reducing the friction velocity. Since it was not practical to increase the kinematic viscosity, or to use a more-viscous fluid than air, the tunnel was designed to produce a fully turbulent boundary layer with as low a friction velocity as possible. This was done by reducing the freestream velocity in the wind tunnel.

Because the speed is low, and a fully turbulent boundary layer at large Reynolds number is desired, a long region for streamwise development of the boundary layer is required without transverse contamination from the sidewalls. Sidewall contamination was eliminated by construing a long, straight wind tunnel with a circular cross-section. The investigation of the structure of small-scale turbulence to be described in this paper is limited to the region very near the wall, so that the distance from the wall is small compared to the boundary-layer thickness and the radius of the tube. This ensures that any effect of transverse curvature of the wall on the structure of turbulence in the wall region will be small.

The wind tunnel, shown schematically in figure 1, consists of an 18.3 m long tube, 0.76 m in diameter, fabricated from smooth sheets of aluminium alloy 1.32 mm thick. The sheets were fastened together with an epoxy adhesive (3M Structural Adhesive 2216). Each sheet was rolled into a tube, 1.22 m long, and all the interior joints were smooth joints made with the edges of the aluminium sheet 'butted' together. The method of fabrication, support, and alignment of the wind tunnel is described by Sharma (1980). The axis of the completed tube was straight to within 3 mm and the inside diameter of the tube did not vary by more than 1 mm. Each joint was carefully smoothed and any imperfections on the inside of the tube were filled with epoxy and sanded until smooth.

A bellmouth section was fitted on the entrance of the tube. A honeycomb, made from plastic drinking straws resting against a 12 mesh per cm stainless-steel screen 20 cm downstream of the tube entrance, was used to smooth and remove large-scale vorticity from the entering air flow. A sealed chamber containing the hot-wire probes and other instrumentation was fitted over the downstream end of the tube. Flow in the tunnel was produced with a centrifugal fan powered by an electrically driven variable-speed transmission. The fan was used to withdraw air from the rear of the sealed chamber in a direction along the extension of the tube axis.

2.2. *Hot-wire anemometer probes*

Initial measurements of the streamwise velocity were made using hot wires of either 3.75 μm or 0.5 μm diameter and various sensing lengths. The wire used was manu-

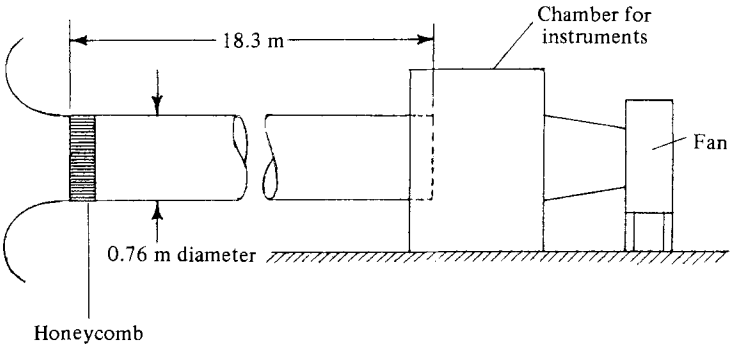

FIGURE 1. Sketch of wind tunnel.

factured by the Wollaston process and was an alloy of 90% platinum and 10% rhodium, covered with a thick coating of silver. For sensing lengths greater than 100 μm the sensors were fabricated in the manner described by Willmarth *et al.* (1976). The smaller sensors (sensing length approximately 25 μm) were fabricated, initially, by bending a length of Wollaston wire into the shape of a hairpin, soldering one leg to a needle, and bonding the other leg to another needle, 2 mm distant from the first, with conducting epoxy. The silver coating of the hairpin-shaped wire was then reduced in diameter and tapered along the legs of the hairpin by electropolishing (i.e. reverse plating of the silver coating). The tapered wire was next coated with a positive-acting photoresist and allowed to dry in an oven. The centre of the coated wire, at the head of the hairpin, was then exposed to a collimated beam of ultraviolet light 20 μm wide. The exposed photoresist was removed in a developer, resulting in a 20 μm wide region of uncoated silver near the centre of the head of the hairpin. The silver in that region was removed by continuing the electropolishing process until the platinum–rhodium wire was exposed.

This method of fabrication was reliable when the prongs formed by the tapered hairpin were 2 mm apart. However, when the prong spacing was reduced to 0.5 mm the hot-wire sensors broke after the final electropolishing process. Failure was attributed to increased bending stress in the wire. A new method was developed involving both electropolishing and electroplating. A hairpin-shaped wire was formed and attached to needles with the hairpin legs 0.5 mm apart. The hairpin-shaped wire was tapered as described above, and the tip of the hairpin was immersed in the electropolishing solution. Electropolishing was then continued until the Pt–Rh wire at the head of the hairpin was exposed. The exposed wire, approximately 400 μm long, did not break since the length was large compared with the diameter, and residual stresses could be accommodated. The probe body was mounted in a micromanipulator with the plane formed by the prongs vertical and the axis of the probe at a 45° angle to the vertical. The Pt–Rh wire was positioned in the electroplating solution so that half of the bare Pt–Rh wire was immersed. Silver was plated on the wire until the diameter was approximately 10–15 μm. Next the probe was rotated 180° about the probe axis. The other half of the exposed Pt–Rh wire was immersed in the plating solution until approximately 20 μm of the bare Pt–Rh wire remained above the solution. The submerged portion of the wire was then plated with silver as described above. In all cases probes constructed with lengths less than 400 μm had sensor diameters of 0.5 μm, while the longer probes were made from wire with a diameter of 3.75 μm.

2.3. *Hot-wire traversing mechanism*

In order to position the hot wires in relation to the wall, a traversing mechanism (Uni-Slide) was mounted just downstream of the end of the tube in the sealed chamber. The hot-wire probe was clamped to a small, upstream-extending, streamlined support. This support was in turn bolted to the traversing mechanism. The hot wire could be positioned with an accuracy of the order of 25 μm at distances from 0 to 20 cm from the wall and 30.48 cm from the end of the tube.

Measurements were also made with two hot wires. However, owing to the limitations of time and expense, it was not possible to construct a traversing mechanism capable of precisely positioning both probes 30.48 cm from the end of the tube. Instead, a commercially available micromanipulator (Hacker Instruments, Model M1), mounted outside the end of the tube, was used to hold and position the hot-wire probe closest to the wall. This probe extended 7.62 cm upstream from the tube end. The other hot wire was mounted on the Uni-Slide mechanism described above and also positioned 7.62 cm from the end of the tube.

The position of a hot-wire sensor, relative to the wall, was established by measurement of the distance between the image of the sensor and its reflection from a polished section of the tube wall using a microscope fitted with a filar eyepiece.

2.4. *Hot-wire-anemometer operation, electronics systems and data acquisition*

The sensitivity of low-aspect-ratio hot wires to the fluid velocity is much less than for high-aspect-ratio hot wires of the same diameter. When the aspect ratio of the hot wire is low, a relatively large fraction of the heat supplied to the wire by the heating current is lost by conduction to the supporting prongs. In order to obtain as large a signal-to-noise ratio as possible, the wires were heated using the constant-current mode of operation.

Betchov (1952) and Kronauer (1953) have studied the effect of aspect ratio on the sensitivity of hot wires operated in the constant-current mode. They assumed that the temperature of the supporting prongs was constant. Sharma (1980) extended Betchov's nonlinear numerical results to include the case of very small aspect ratio, when the heat loss to the supporting prongs is larger than the heat loss to the fluid. He made calculations, based on Betchov's work, of the static and dynamic sensitivity of 0.5 μm diameter platinum hot wires operated with an overheat ratio of 0.5 for aspect ratios as low as 32. The calculations showed that the static sensitivity for an aspect ratio of 32 was $\frac{1}{6}$ of the sensitivity for the same-diameter wire of infinite aspect ratio. The temperature distribution was far from uniform, with low-temperature regions near each supporting prong, and a short, but very hot, central region that is required in order that the average temperature of the wire be 50 % greater than the ambient temperature.

The assumption of constant temperature of the supporting prongs for the low-aspect-ratio hot wires constructed for this investigation is valid. A rough estimate, based on heat conduction from the wire to the prongs, of the temperature change along the length of the relatively massive 20 μm diameter silver supporting prongs gave a temperature change of only 0.5 % of the hottest central portion of the hot wire. Thus the prong temperature adjacent to the hot wire can be, at most, only a degree above the ambient temperature of the flow. This, coupled with the fact that silver supporting prongs have a very low resistance compared with the resistance of the hot wire, of the order of 0.5 % of the hot-wire resistance, and a much lower thermal coefficient of resistance than the hot wire, of the order of $\frac{1}{6}$ of the thermal coefficient

of resistivity of the hot-wire material, has the result that a negligible signal will be produced as a result of any velocity variation over the prongs of the low-aspect-ratio hot wires.

Since there is a relatively large amount of heat transferred by conduction along the hot wire to the supporting prongs, the sensitivitiy of the hot wire to changes in the flow velocity is greatly reduced. Relative to a high-aspect-ratio hot wire, there is less heat available for sensing the velocity by thermal convection to the flow, and the hottest, most-sensitive, portion of the wire is smaller fraction of the total length of the wire.

Although the sensitivity of a small-aspect-ratio hot wire is very low, the change in the sensitivity as a function of frequency turns out to be less than it is for a larger-aspect-ratio hot wire (i.e. the frequency response of a short hot wire is better than for a long hot wire). Calculations of the dynamic sensitivity for a 0.5 μm diameter wire with an aspect ratio of 32 revealed that the frequency response is constant to within 1 db for frequencies up to 10 kHz. For infinite aspect ratio, with the same-diameter wire, 3 db attenuation of the signal occurs at approximately 5 kHz. The results of the extension of Betchov's numerical, static and dynamic calculations to lower aspect ratios were found to be in agreement with the linearized calculations made by Kronauer (1953). This is described in greater detail in Sharma (1980).

The constant-current anemometer circuit used for the small-diameter hot wires was a Wheatstone bridge with the hot wire in one arm of the bridge. The bridge was connected in series with a low-noise voltage source and a large resistance. The bridge imbalance was sensed with a differential amplifier (Teledyne Philbrick Model 4523). The large-diameter hot wires were powered with a constant-current linearized anemometer (TSI model 1054B). Preliminary examination of the analog signals produced by both large- and small-aspect-ratio hot wires in the flow facility described above revealed that there was negligible energy in the frequency spectrum above 1 or 2 kHz; frequency compensation for the small-diameter hot wires was not necessary.

The hot-wire signals were amplified and the d.c. levels shifted as necessary with signal conditioners employing operational amplifiers (Analog Devices Model 45). The amplified signals were recorded over the full dynamic range of a Honeywell Model 5600C 7-channel FM recorder with frequency response from 0 to 5 kHz. The data were played back and analysed using a mini-computer (Data General NOVA 840) interfaced to an 8-channel A/D converter with simultaneous sample and hold inputs (Analogic Model AN5800). The data were digitized at a rate of 10 kHz per channel to prevent aliasing of the signals as described by the Nyquist condition. (10 kHz is twice the frequency at which the signals are low-pass filtered by the rapid drop in the frequency response of the tape recorder.) Actually, aliasing was not a problem since none of the analog signals contained significant energy or noise above 1–2 kHz. Power-spectral-density measurements of the tape-recorded data were made with a Hewlett-Packard Spectrum Analyser Model 3580A.

3. Calibration of the hot wires and wind tunnel

Improvements in the method of fabrication of the small hot wires, the tunnel calibration, and the initial measurements using the small hot wires in the tunnel were carried out at the same time. Before the initial measurements were made, a porous plastic filter, one centimetre thick, was installed over the bellmouth contraction to

remove dust and dirt from the air in the hope that the life of the hot wires would be increased. It was found that the pressure drop through the filter was not uniform, which caused the mean flow in the tunnel to be very non-uniform. Removing the filter improved the flow, but probably also decreased the life of the hot wires. When the filter was removed we noticed that the plastic drinking straws, used as a honeycomb in the entrance region of the pipe, had become somewhat compacted under their own weight. A small open region at the top of the tube was present, and this was filled with additional straws.

Owing to the low sensitivity of the small hot wires it was necessary to employ high-gain amplifiers with frequency response from 0 to 5 kHz and adjustable bias voltage. Typicaly a gain of 1000 was required. The amplifier signals would often drift away from the desired voltage that had been set after the initial overheat ratio and bias voltage adjustment. Voltage drift was a serious problem, and, when it was too great, the offending hot wire would have to be discarded. This was not a trivial matter, since construction of a new hot wire required a day (often longer when difficulties were encountered). The cause of the drift was never definitely established; however there are two probable causes: incomplete cleaning of etched wires and/or electromigration. Willmarth & Bogar (1977) were unable to remove the etching solution completely from their small hot wires, and after a few weeks slow corrosion of the silver coating always occurred. Black (1969) has presented a survey of the phenomenon of electromigration, and Hummel & Breitling (1971) describe measurements of the electromigration of silver. In the latter paper a change in the resistance of a silver film owing to migration of silver atoms at current densities of the order of 7×10^5 A/cm^2 was observed. In recent work with small hot wires, at comparable current densities, Sharma (unpublished) observed migration of the plated silver film onto the exposed platinum wire using an electron microscope.

3.1. *Hot-wire calibration*

Owing to the difficulties with drift of the output voltage of the hot wires, a static calibration was performed after a measurement at each point in the boundary layer. When a useable small hot wire had been fabricated and placed in operation at a given point in the boundary layer, the hot-wire output voltage was recorded on magnetic tape. In this process the overheat ratio, gain and bias voltage of the amplified signal were adjusted so that the full dynamic range of the tape recorder was utilized. Immediately after recording the data (without changing the overheat ratio, gain or bias) the hot wire was positioned on the centreline of the wind tunnel and the speed of the tunnel was slowly varied while the hot-wire output voltage was again recorded over the full dynamic range of the tape recorder. The mean speed of the flow 0.18 m above the tunnel centreline was also measured (using a Gill propeller anemometer) and simultaneously recorded on another channel of the tape recorder. Figure 2 is a typical example of the data recorded during calibration of the hot wire at a given point in the boundary layer. Since the speed of the tunnel during calibration could not be varied without some unsteadiness of the flow and the presence of large-scale intermittency on the tunnel centreline made the hot-wire and propeller-anemometer signals somewhat unsteady, the oscilloscope trace is rather broad, as can be observed in figure 2.

For measurements at each point in the boundary layer, a digital computer program was used to perform a short-time average of the unsteady, slowly varying calibration data, and to construct a 25-entry calibration table of the hot-wire output voltage as a function of velocity measured by the Gill propeller anemometer. Another

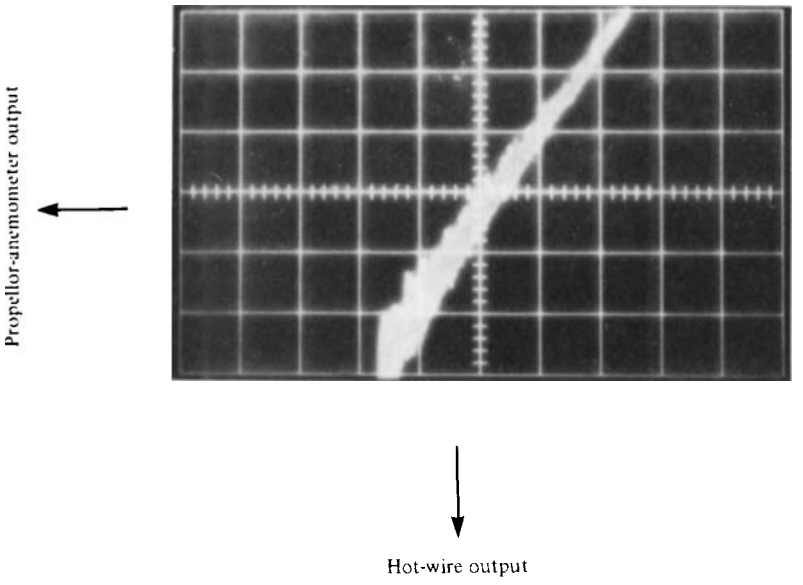

FIGURE 2. Typical calibration trace for small hot wire with gain, bias and overheat ratio adjusted for hot wire located at $y^+ = 13.3$. Storage oscilloscope display. Probe dimensions $l = 30$ μm ($l^+ = 0.39$), $d = 0.5$ μm.

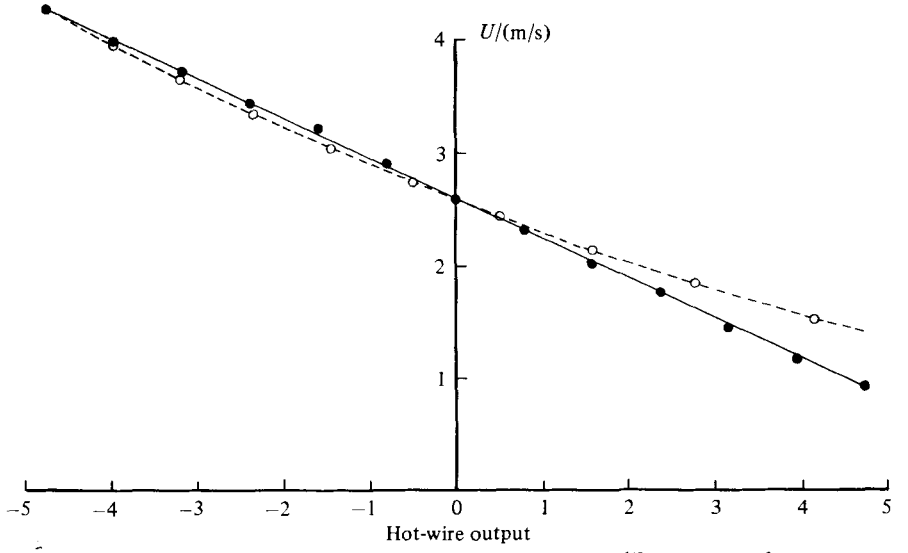

FIGURE 3. Comparison of calculated and experimental calibration results at $y^+ = 13.3$: ○, calculated; ●, experimental.

program was used to determine the velocity measured by the hot wire. This program determined the velocity, for each digitized data point, by interpolation, using the previously generated calibration table.

Numerical results of this calibration procedure for a typical small hot wire of aspect ratio 50, adjusted for measurements within the boundary layer at 13.3 viscous lengths from the wall, are shown in figure 3. Also shown in the figure are numerical results computed using the theory of Betchov (1952) for the same conditions. The agreement

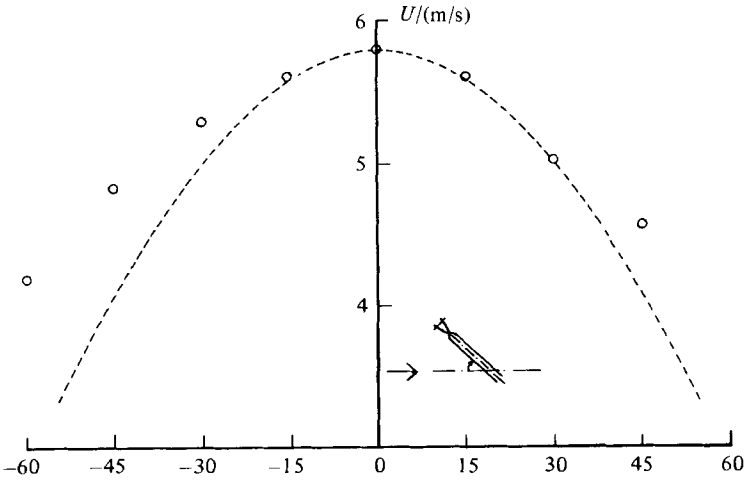

FIGURE 4. Directional sensitivity of small hot wire. Wire dimensions $l = 25$ μm, $d = 0.5$ μm. $U_\infty = 5.79$ m/s. ○, velocity indicated by hot wire; ----, velocity normal to hot wire $= U \cos \alpha$.

between the calculations and measurements is reasonably good. It should be noted that, owing to the reduced sensitivity of the hot wire caused by the large heat transfer to the prongs, the output voltage of the hot wire is approximately linear with respect to velocity.

To ensure that drift of the hot-wire signal had not occurred, the mean value of the hot-wire signals in the boundary layer before and after calibration were checked. If drift had occurred the run was repeated. When the drift could not be eliminated the hot wire was discarded and a new one was constructed.

The directional sensitivity of the low-aspect-ratio hot wires was determined by yawing them on the centreline of the wind tunnel using a mechanism whose axis of rotation passed through the hot wire. The directional sensitivity of a hot wire of aspect ratio 50, measured at speeds between 5.79 and 1.4 m/s, was less than that of an infinite-aspect-ratio hot wire. We did not investigate the directional sensitivity in great detail, because drift of the hot-wire signals made it difficult to collect valid data before a particular wire had to be discarded and a new one constructed. The length and therefore the aspect ratio of the new hot wire could not be precisely controlled. The directional sensitivity at 5.79 m/s, shown in figure 4, is typical of the results at the other speeds. The voltage output variation for an infinite-aspect-ratio hot wire (approximately proportional to the cosine of the yaw angle) is also plotted in figure 4. The directional sensitivity appears to be sufficient to allow the measurements of cross-stream velocity components (provided that the very difficult problem of constructing an array of two or more low-aspect-ratio wires can be solved and that the directional sensitivity is not a significant function of the geometry of the support prongs).

3.2. *Tunnel calibration*

When mean-velocity profiles in a vertical plane from the lower wall to the centreline of the tunnel were measured, the flow on the tunnel centreline was found to be intermittently turbulent. As mentioned in §2, this was caused by occasional large eddies extending well beyond the mean boundary-layer thickness. The primary purpose of this investigation is the study of small-scale turbulence near the wall. Since

the flow field near the wall scales with wall variables and obeys the law of the wall (see §4) the outer part of the boundary layer will not have a significant effect on the small-scale turbulent structure in the region very near the wall. The structure of turbulence, measured by many investigators, in the wall region of boundary layers developed on plane surfaces, in pipes or in channels is essentially the same.

After the measurements of the small-scale turbulent structure near the wall were nearly complete, we discovered a slight asymmetry of the flow in the vertical plane of the tunnel. The mean velocity 0.18 m above the tunnel centreline was 6.5 % higher than the velocity on the tunnel centreline. This asymmetry was caused by non-uniformity of the honeycomb at the entrance of the tunnel, arising from the deformation of the plastic drinking straws used to form the honeycomb. We had already observed a much greater deformation of these straws when the tunnel was constructed (as mentioned in the introduction to this section). Observations of the rotation rate of a small propeller were used to determine the approximate velocity distribution of the flow at the inlet just ahead of the honeycomb and the tunnel exit. It was found that the initial velocity distribution was essentially the same as the final distribution. Observations of the flow direction near the exit of the tunnel with a long thread of yarn showed no evidence of swirl or secondary flow. Since most of the measurements of turbulent structure were made at distances less than fifty viscous lengths from the wall, the effect of the asymmetry of the flow in the vertical plane of the tunnel on the small-scale turbulent structure in the wall region can be neglected. The freestream velocity was taken to be the velocity on the centreline of the tunnel.

4. Measurements of mean and fluctuating velocity with a single probe

4.1. *Mean-velocity profiles*

Measurements of the mean velocity in the boundary layer in the new flow facility were made with hot wires of two different lengths on the lower wall 30.48 cm from the end of the tube. The hot wires were calibrated at each point in the measured profile, as explained in §3.1. Note that buoyancy effects on the hot-wire response can be neglected because the typical Grashof number is less than the cube of the Reynolds number, based on wire diameter (see Collis & Williams 1959).

Figure 5 shows the velocity profiles measured with two hot-wire probes 425 μm and 200 μm long for two different tunnel speeds. The velocity measured at $y^+ = 1.8$ may be slightly affected by heat transfer to the wall since the ratio of distance from the wall to hot-wire diameter is less than 100 (see Wills 1962). The solid line on figure 5 is the velocity profile in the wall region of the ideal turbulent boundary layer on a flat plate when the pressure gradient is zero, as described by Coles (1955). The measured profiles are in agreement with the ideal profile proposed by Coles out to distances from the wall of the order of 1000 viscous lengths.

The boundary-layer displacement and momentum thickness were calculated from the velocity profiles of figure 5. These and other mean-flow boundary-layer parameters are tabulated in table 1. Also displayed in table 1 are Coles' (1955) parameters for the ideal turbulent boundary layer on a flat plate at the same values of u_τ/U_∞. The mean-flow parameters are in substantial agreement with those of an ideal turbulent boundary layer.

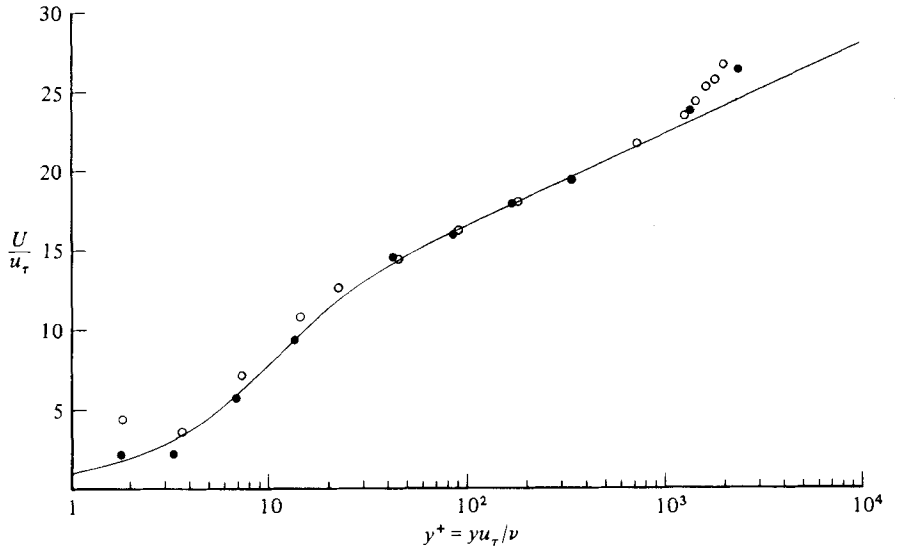

FIGURE 5. Mean-velocity profiles at 30.48 cm from the end of the tunnel: ○, $u_\tau = 11.5$ cm/s ($l = 425$ μm, $U_\infty = 3.05$ m/s); ●, $u_\tau = 21$ cm/s ($l = 200$ μm, $U_\infty = 5.79$ m/s).

	U_∞ (m/s)	Re_θ	δ (m)	δ^* (m)	θ (m)	$\frac{\delta^*}{\theta}$	$\frac{u_\tau}{U_\infty}$	Re_x ($\times 10^{-6}$)
Present work	3.05	6480	0.279	0.0463	0.0340	1.362	0.0377	3.43
Coles' ideal boundary layer	—	5130	—	—	—	1.370	0.0377	3.03
Present work	5.79	9840	0.229	0.0349	0.0255	1.366	0.0363	6.94
Coles' ideal boundary layer	—	8007	—	—	—	1.351	0.0363	5.15

TABLE 1. Properties of the actual and ideal turbulent boundary layer

4.2. *Measurements of the root-mean-square and power spectra of the streamwise velocity fluctuations*

In addition to the mean velocity, the streamwise velocity fluctuations were measured 30.48 cm upstream of the end of the tube for a number of different locations. Figure 6 is a plot of the root-mean-square (r.m.s.) velocity fluctuation, u', profiles measured with two hot-wire probes 30 μm and 200 μm long (i.e. 0.375 and 2.5 viscous lengths). The measurements show considerable scatter but are generally in good agreement with the data of Klebanoff (1954), shown by the dashed line. One should note that there is no obvious increase in the value of u'/U_∞ measured with the small wires when compared with Klebanoff's (1954) data. Bull & Thomas (1976) observed a significant increase (50 %) in the r.m.s. wall pressure when the diameter of their small pressure transducers was reduced from 200 to 30 viscous lengths. Klebanoff's (1954) data were obtained using 500 μm long wires in a flow where the wire length was 17 viscous lengths. The increase in the r.m.s. wall pressure observed by Bull & Thomas (1976) when the diameter of their transducers was reduced was approximately linear and only increased by 5 % when the transducer diameter change was 16 viscous lengths.

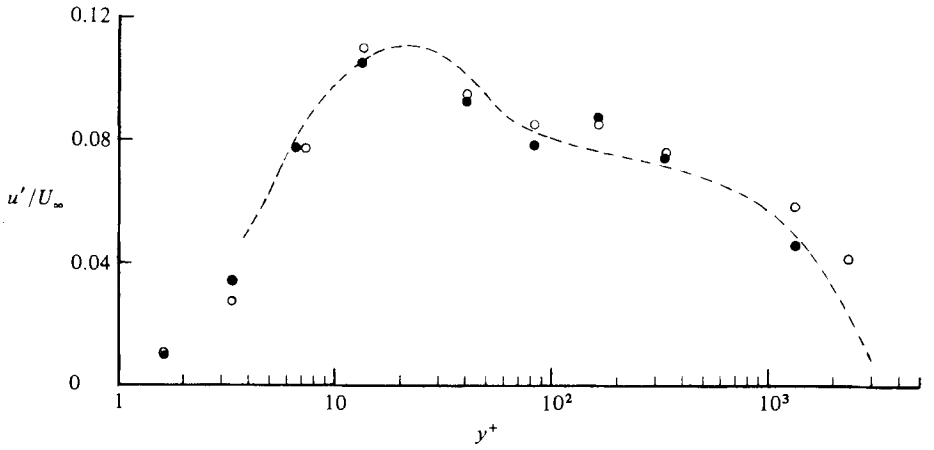

FIGURE 6. Streamwise turbulent intensity profiles; $U_\infty = 5.79$ m/s: ●, $l = 30$ μm, $d = 0.5$ μm; ○, $l = 200$ μm, $d = 0.5$ μm; ----, Klebanoff (1954).

Thus it is not surprising that little change is observed in figure 6 between the present data and Klebanoff's (1954) data.

The power spectra of the streamwise velocity fluctuations was measured using different-length hot wires under identical conditions at a distance of 13.3 viscous lengths from the wall and 30.48 cm upstream from the end of the tube. Three hot wires were used to make the measurements: one with commercially available dimensions, $l = 850$ μm and $d = 3.75$ μm, and two 0.5 μm diameter hot wires, one 200 μm long and the other 30 μm long.

To display the effect of hot-wire length on the power spectral density, the spectra $\phi(\omega)$ of the signals from each hot wire were normalized so that on a plot of spectral density versus frequency (scaled with the viscous time ν/u_τ^2) the areas beneath the normalized spectra were unity. The normalized spectra are shown in figure 7. At the higher frequencies the normalized spectral density of the signal from the shortest hot wire is approximately five times as large as that measured by the longest hot wire. The length of the shortest hot wire was approximately 0.4 viscous lengths and that of the longest hot wire was approximately 12 viscous lengths. The increased high-frequency power-spectral density of the signal from the shortest hot wire demonstrates that the small-scale velocity fluctuations in the region near the wall are as small as, or smaller than, the viscous length.

4.3. *Estimate of the small-scale structure resolved by hot wires of various lengths at 13.3 viscous lengths from the wall*

Then normalized power spectra of figure 7 were used to determine the fraction of the root-mean-square streamwise velocity fluctuations resolved by hot wires of a given length. At low frequencies the long and short hot wires correctly resolve the power spectra of the velocity fluctuations, and the low-frequency power-spectral density is the same for each hot wire. The normalized power spectra for the two shorter hot wires were multiplied by constant values so that at low frequencies the spectral density was the same as that measured by the longest hot wire. The area beneath each of the spectra is now proportional to the mean-square velocity measured by each hot wire.

The area beneath each of these power spectra was plotted as a function of hot-wire

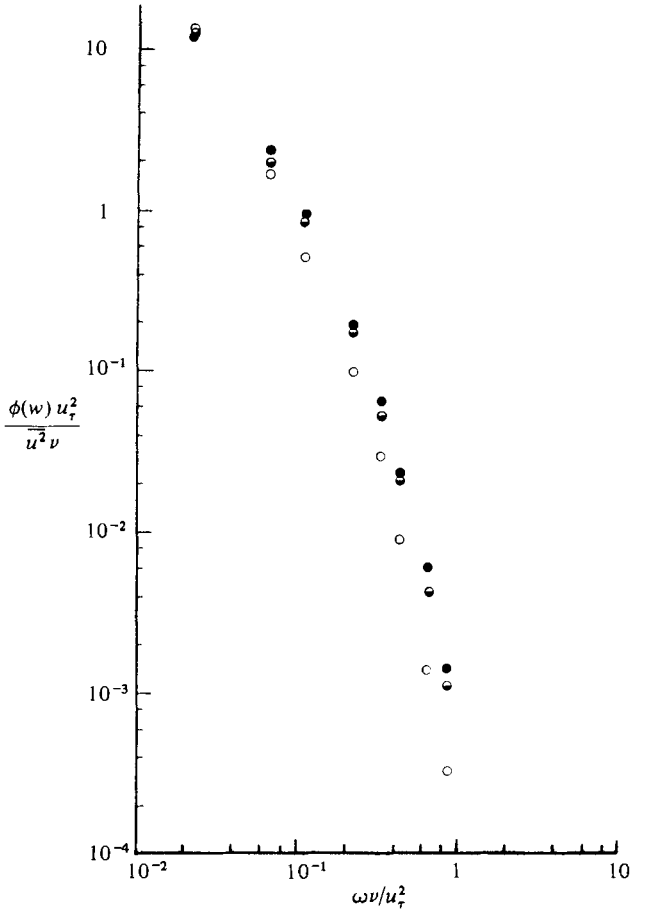

FIGURE 7. Normalized power-spectral density of streamwise velocity fluctuations for hot wires of various lengths at $y^+ = 13.3$ and $U_\infty = 5.79$ m/s: ●, $l = 30$ μm, $d = 0.5$ μm; ◒, 200 μm, 0.5 μm; ○, 850 μm, 3.75 μm.

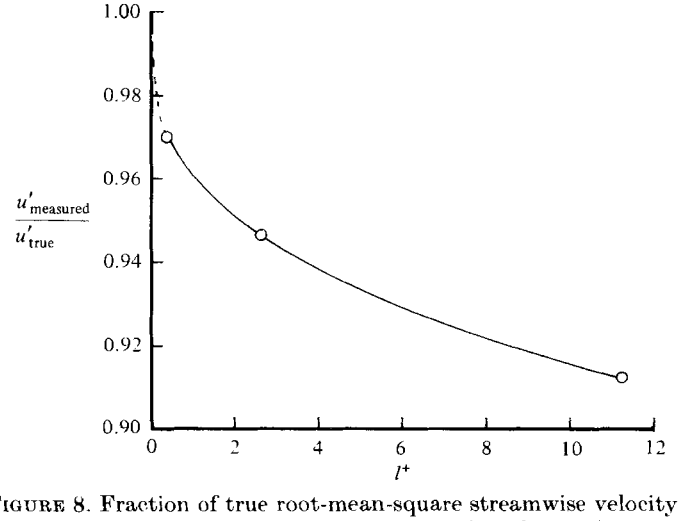

FIGURE 8. Fraction of true root-mean-square streamwise velocity fluctuations measured by hot wires of various lengths at $y^+ = 13.3$.

length. Then a curve was faired between the three points, and the approximate intercept at zero hot-wire length was estimated. The value of the ordinate (an area) at the intercept is proportional to the mean-square velocity that would be measured by a hot wire of zero length. Figure 8, the square root of the area beneath each of the spectra divided by the square root of the area at the above intercept plotted as a function of dimensionless hot-wire length, shows the attenuation of the root-mean-square velocity caused by hot-wire length at a distance of 13.3 viscous lengths from the wall. It can be seen from the figure that the longest hot wire (which was 850 μm long, or 10.3 viscous lengths) was unable to resolve approximately 20 % of the mean-square velocity fluctuations (10 % of the root-mean-square velocity fluctuations). This implies that there is small-scale turbulence amounting to roughly 20 % of the turbulent energy in the boundary layer near the wall, which was heretofore unaccounted for because the measuring probes were too large.

5. Measurements of the frequency of bursting

In an effort to determine a scaling law for the frequency of bursting, Narahari Rao, Narasimha & Badri Narayanan (1971) measured streamwise velocity fluctuations in the boundary layer with a hot wire. The occurrence of large-amplitude fluctuations of bandpass-filtered hot-wire signals were used to detect bursts. Although they reported some problems with the identification of bursts, their results indicated that the burst frequency scales with the timescale of the outer flow δ/U_∞, rather than with the viscous timescale ν/u_τ^2. The result was compatible with the results reported by Kim *et al.* (1971), which were obtained in a flow at much lower Reynolds number. Additional support for this scaling law was given by Laufer & Badri Narayanan (1971), who pointed out that the mean frequency of the bursts was of the same order as that of the turbulent bulges in the outer intermittent region of the boundary layer. Kovasznay, Kibens & Blackwelder (1970) have also suggested that bursts in the region near the wall could have some relation to the turbulent bulges in the outer flow.

5.1. *Method of burst detection*

Measurements of the frequency of bursting were made using the small hot wires developed for the present investigation. The detection of bursts should be improved as a result of the better spatial resolution of the small hot wires, which, as has been shown above, sense additional small-scale turbulence. Many methods have been used to detect bursts, with varying degrees of success. In every case the results obtained with a given method of burst detection depend upon the detection criteria and parameters. For the present measurements we used the VITA method of burst detection devised by Blackwelder & Kaplan (1976) with the addition of a slope detection criteria suggested by the work of Chen & Blackwelder (1978). We also used exactly the same burst detection criteria and parameters that were used by Chen and Blackwelder (1978), and more recently by Blackwelder & Haritonidis (1983), in order that valid relative comparisons could be made between their results and our results. We realized that the VITA method of burst detection may not be perfect, but by comparing bursting statistics measured with exactly the same criteria and parameters valid comparisons of changes in burst frequencies and the dependence on scaling laws can be determined.

To identify a burst, Blackwelder & Kaplan (1976) calculated the short-time variance relative to the short-time mean of the streamwise velocity fluctuations

measured at a distance of 15 viscous lengths from the wall. They called this the variable-interval time-averaging (VITA) technique. For burst detection they used a time-averaging interval of 10 viscous timescales ($T = 10\nu/u_\tau^2$). Their criterion for burst detection was that the above short-time variance of the velocity fluctuations relative to the short-time mean be greater than the long-time variance of the velocity fluctuations. In other words, using the VITA technique, a burst is identified when the short-time average streamwise turbulent kinetic energy relative to the short-time average streamwise velocity exceeds the long-time average streamwise turbulent kinetic energy. This is in agreement with the burst detection methods of Narahari Rao *et al.* (1971), the visual studies of Kline *et al.* (1967), and Corino & Brodkey's (1969) observation that, during a short-time interval, intense high-frequency turbulence was associated with a burst.

Chen & Blackwelder (1978) found that the more important aspects of the bursting phenomenon occurred primarily when the fluid was accelerating. Blackwelder (1979 private communication) added the criterion to their burst-detection algorithm that when a burst occurs the streamwise velocity must be increasing with time, i.e. $\mathrm{d}u/\mathrm{d}t$ must be positive at the centre of the short time interval. When this criterion and the above criterion, that the short-time variance (relative to the short-time mean) of the streamwise velocity exceeded the long-time variance of the streamwise velocity, a burst was deemed to have occurred. The burst was over once either of the above criteria was no longer satisfied.

The computer program that we used was identical (except for one change to be described below) to the one used by the University of Southern California group and was obtained from Blackwelder. The program also saved the digitized data, both preceding and following a burst, for later analysis.

After analysing our initial data using the above VITA technique, we found that the algorithm occasionally found multiple bursts. This occurred because the streamwise velocity during a burst would sometimes have small 'bumps' in it, i.e. the velocity would not be continuously increasing near the centre of the short-time averaging interval, but would have one or more small decreases in velocity followed by a generally increasing velocity. Some bursts had as many as four such 'bumps'. Whenever a 'bump' was encountered during a burst, the slope $\mathrm{d}u/\mathrm{d}t$ would become negative for a short time even though the short-time variance was still greater than the long-time variance. Hence the program would signal the end of a burst, and then the burst-detection scheme would find yet another burst once the centre of the short-time averaging interval had advanced beyond the 'bump'.

In order to avoid the detection of multiple bursts during the short-time averaging interval, the program was changed so that when a burst was first detected the detection criteria were 'switched off' for the data that followed the burst. The 'switch-off' period lasted for a time equal to the short-time averaging interval. This change in the algorithm reduced the burst frequency, but never by more than 15%.

5.2. *Measurements of bursts using the VITA method*

Measurements of the burst frequency were made 7.62 cm from the end of the tube with two hot wires placed a few viscous lengths apart and mounted on separate traversing mechanisms. The measurements with two hot wires are discussed in §6. We were concerned that the effects of the end conditions of the tube might alter the small-scale structure of the turbulence near the wall and hence the burst frequency. Measurements were made of the power spectra of the streamwise velocity fluctuations and of the burst frequency using a single hot wire placed 7.62 cm and 30.48 cm from the end of the tube.

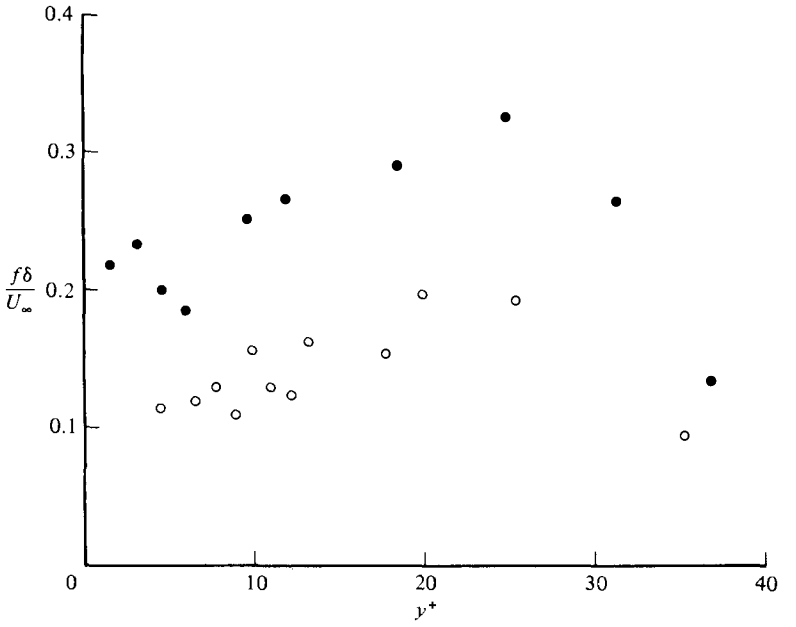

FIGURE 9. Dimensionless burst frequency scaled with respect to outer flow variables, as a function of Reynolds number and distance from the wall: ●, $Re_\theta = 9840$; ○, $Re_\theta = 6480$.

We found that the only effect of the tube end conditions on the power-spectral density of the velocity fluctuations was to increase the low-frequency power-spectral density at a distance of 1.6 and 3.6 viscous lengths from the wall. The high-frequency power-spectral density 1.6 and 3.6 viscous lengths from the wall was not affected by the end conditions. Further from the wall, out to distances of the order of 50 viscous lengths, the end conditions had no effect on the power-spectral density. The burst frequencies from the wall out to distances of the order of 50 viscous lengths were measured and it was found that the burst frequencies were not affected by the end conditions. This is not surprising, because the VITA method of burst detection is primarily sensitive to the occurrence of intense high-frequency components of the velocity fluctuations. For additional information concerning these measurements see Sharma (1980).

The streamwise velocity data used for burst detection were obtained using a 0.5 μm diameter 25 μm long hot wire mounted 7.62 cm from the end of the tube and traversed normally to the wall. The hot-wire signal was recorded and later digitized at a rate of 10 kHz. Since the hot-wire signal varies approximately linearly with velocity, it was not necessary to use the computer to linearize the signals. We did compare data that was linearized by computer with data that was not linearized, and found no difference in the root-mean-square velocity or the burst frequency. Thus it was not necessary to perform the lengthy hot-wire calibration procedure for these measurements.

The burst frequency was measured as described in §5.1 and was found to increase slowly as the hot wire was moved away from the wall. A maximum frequency was reached approximately 25 viscous lengths from the wall and then the burst frequency rapidly decreased. The results of these measurements of the burst frequency, scaled with outer variables (i.e. the outer timescale δ/U_∞), at two speeds are displayed in figure 9. Figure 10 shows the same data, scaled with wall variables (i.e. the viscous

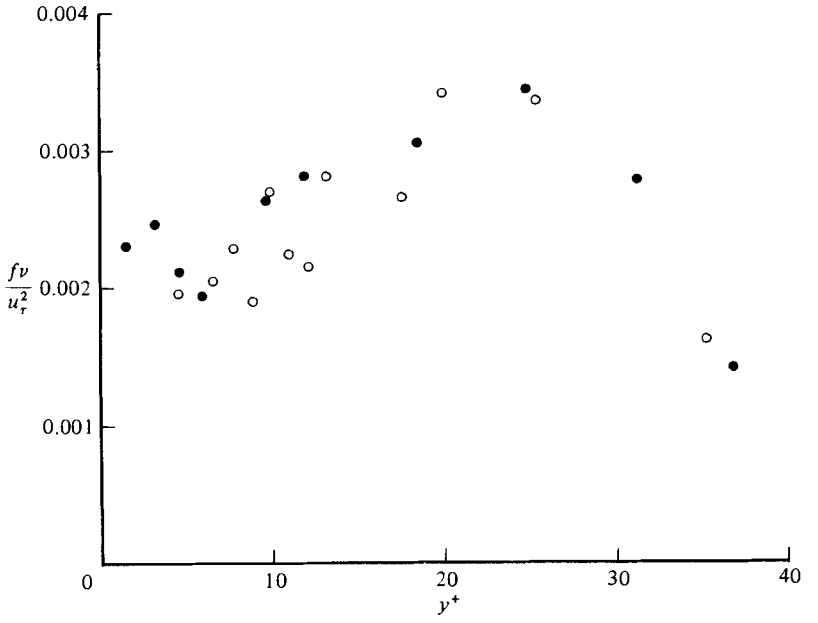

FIGURE 10. Dimensionless burst frequency scaled with respect to wall variables, as a function of Reynolds number and distance from the wall: ●, $Re_\Theta = 9840$; ○, $Re_\Theta = 6480$.

timescale ν/u_τ^2). It is clear that the bursting frequency scaled with the outer timescale increases with the Reynolds number. On the other hand, the burst frequency scaled with wall variables is constant with respect to Reynolds number. This is consistent with the recent work of Blackwelder & Haritonidis (1983), who found that the burst frequency measured with very short hot wires was independent of Reynolds number when scaled with the viscous timescale. Figure 11 and 12 are plots of our measurements of the burst frequency and the measurements of Blackwelder & Haritonidis at a distance of 15 viscous lengths from the wall. The burst-frequency data of figure 11 are scaled with the outer timescale, and the data of figure 12 are scaled with the viscous timescale. The burst frequency scaled with the viscous timescale is independent of Reynolds number and has almost the same value as measured by Blackwelder & Haritonidis.

Sharma (1980) found that when the length of the hot wire was increased from 0.375 to 2.5 viscous lengths the burst frequency was not significantly different. This is in agreement with the findings of Blackwelder & Haritonidis, who report a decrease in the burst frequency, scaled with the viscous timescale, which is not significant until the hot-wire length is greater than 5 viscous lengths.

One should note that the burst frequency determined using the VITA technique is extremely sensitive to the threshold level used for the detection algorithm and to the value of the time used to calculate the short-time average. Sharma found a 40 % change in burst frequency when the threshold level for burst detection was changed by 5 %, and a 15 % change in burst frequency when the short-time averaging time $T = 10\nu/u_\tau^2$ was changed by 20 %.

The flow investigated by Blackwelder & Haritonidis was a relatively thin tripped boundary layer. The present flow was a boundary layer developed on a long smooth surface at low velocities over a long distance resulting in approximately the same Reynolds number. When one considers the above sensitivity of the detection

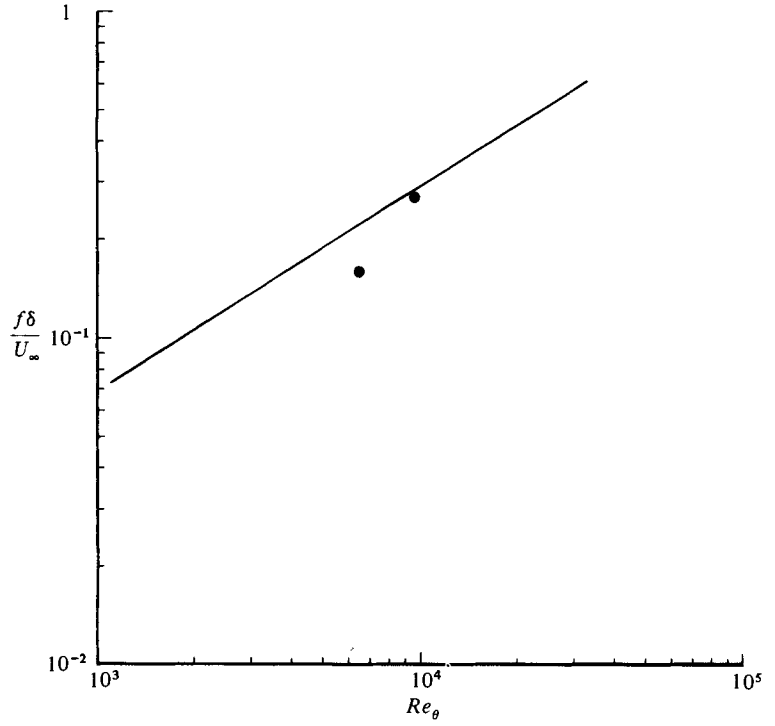

FIGURE 11. Dimensionless burst frequency at $y^+ = 15$ scaled with respect to outer variables as a function of Reynolds number: ----, Blackwelder (1982).

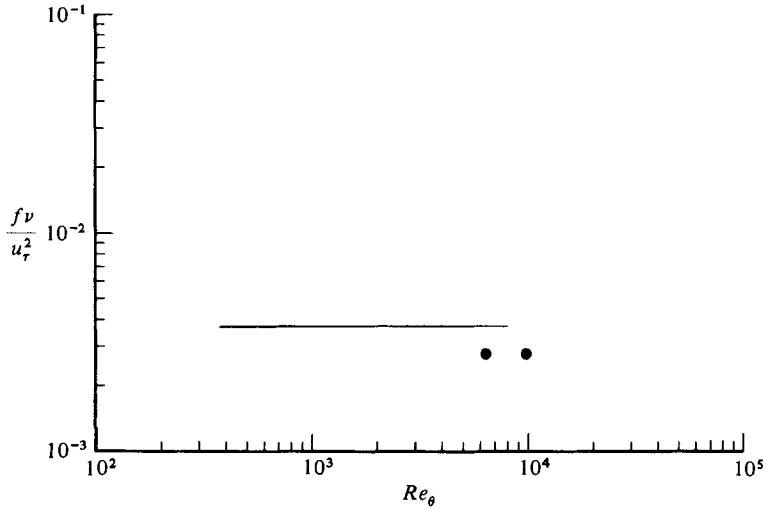

FIGURE 12. Dimensionless burst frequency at $y^+ = 15$ scaled with respect to wall variables as a function of Reynolds number: ----, Blackwelder (1982).

algorithm and the difference between the flows, the agreement between the burst frequencies measured in the two flows is remarkable. It is also encouraging, because it suggests that the VITA technique for burst detection is a worthwhile method that could be used by other investigators to provide more data on the bursting process and for comparison with the present results. Of course one must be certain that the same detection parameters are used.

6. Measurements of small-scale turbulent structure with two hot wires

Willmarth & Bogar (1977) used very small hot wires in an X-array, which was calibrated in a uniform flow, to make velocity measurements in the wall region of a turbulent boundary layer at a Reynolds number of 11 700 based on momentum thickness. As explained in §1, they found that, when small-scale turbulence was present, it was not possible to make accurate measurements of the streamwise and cross-stream velocity components using this measurement technique. Their explanation for this difficulty was that small-scale shear layers in the turbulence caused a significant difference in the velocity to which each hot wire was exposed. This implies that the small-scale turbulent structure had a significant velocity variation over a distance of the order of the hot-wire spacing, which was 2.5 viscous lengths. The length of the hot wires used in the present investigation is less than half the viscous length, so tht the spatial resolution that can be obtained is nearly an order of magnitude better than was realized by Willmarth & Bogar. Further study of the small-scale structure detected by Willmarth & Bogar should be possible using a pair of the small hot wires developed in this investigation.

Measurements were made with two hot wires positioned as closely as possible to each other and near the wall. Aerodynamic interference between the hot wires was as small as possible. The body of each probe was long and slender. The 80 μm Wollaston wire that formed the supporting prongs was also tapered down to 20 μm diameter near the sensing length. Since the support needles, to which the Wollaston-wire prongs were soldered, were more than 1000 μm downstream, aerodynamic interference between the wires should be minimal. The hot wires were each 25 μm long and 0.5 μm in diameter and were mounted parallel to the wall, 7.62 cm upstream from the end of the tube on separate traversing mechanisms, as described in §2.3. Unfortunately it was not possible to make measurements with the hot wires very near the wall when the length of the hot wire was oriented in a direction normal to the wall because the distance between a supporting prong and the sensitive region of the hot wire was too great.

Simultaneous signals from two hot wires parallel to the wall and spaced approximately two viscous lengths apart at various distances from the wall were digitized for 16 s at a rate of 10 kHz and stored on magnetic tape for detailed analysis. An absolute velocity calibration of the hot wires was not necessary since the hot-wire response to velocity is approximately linear.

Measurements were made of the conventional long-time spatial correlation of the streamwise velocity fluctuations when the distance between the hot wires was varied in the spanwise direction and in the direction normal to the wall. The minimum spacing between the wires (in a direction normal to the wall) was approximately one viscous length. As expected, the measurements confirm that the spatial scale of the velocity fluctuations increases with distance from the wall. The correlation coefficients measured for very small spatial separations were large, slightly less than one, and decreased gradually as the spatial separation increased. The results (see Sharma 1980) were in agreement with previous measurements at larger spatial separations that have been reported by Gupta, Laufer & Kaplan (1971) and by Kastrinakis (1971). The measured values of the correlation give accurate data for the rate of decay of the spatial correlation when the spatial separation is small. Using a spatial Fourier transform, the measurements could have been analysed to determine the high-wavenumber spectral density for the wavenumber components normal and parallel to the wall. Owing to the lack of time and resources we did not perform this analysis.

With the aid of a dual-beam storage oscilloscope an examination was made of the signals from two hot wires placed within or above the sublayer when one hot wire was directly above the other. The two signals were found to be generally in phase, but on occasion there were significant differences between them which were of short duration. The intermittent differences in the signals were caused by small-scale shear layers (i.e. small-scale velocity gradients) in the region near the wall. A method for computer analysis of the data to study intermittent fluctuations of the velocity gradient was devised. The method, which is described below, is based upon some of the properties of the velocity fluctuations in the sublayer and in the wall region.

6.1. *Method of analysis of data from two closely spaced hot wires*

In the wall region, for distances greater than 15 viscous lengths from the wall, the intensity of the streamwise velocity fluctuations is relatively constant and decays slowly as the distance from the wall increases. Since the gradient in the intensity of the fluctuations is small, a pair of hot wires in this region, separated in the direction normal to the wall by a small distance of the order of two viscous lengths, will produce approximately the same velocity signal, as a function of time, if the scale of the turbulence is larger than the wire length and spacing. But, when small-scale turbulence is present, the signals will be significantly different.

In the viscous sublayer, at distances less than 5 viscous lengths from the wall, the streamwise velocity fluctuations have been shown to be approximately in phase and with an amplitude proportional to the distance from the wall (see Eckelmann 1974). An approximate expression for the streamwise velocity fluctuations in the sublayer for $y^+ < 5$ is

$$u(y, t) = yf(t), \tag{6.1}$$

where $f(t)$ is a random function of time. In order words the streamwise velocity fluctuations are an unsteady linear function of distance from the wall. Differentiating (6.1) with respect to y yields

$$\partial u/\partial y = f(t). \tag{6.2}$$

Above the viscous sublayer Eckelmann (1974) found that the streamwise velocity fluctuations were no longer in phase. However, in the entire region from the wall out to a distance of the order of 10 viscous lengths from the wall (somewhat before the maximum intensity of the streamwise velocity fluctuations occur) the root-mean-square velocity increases approximately linearly with distance from the wall. A pair of hot wires in this region that are two viscous lengths apart, in a direction normal to the wall, will have root-mean-square velocities considerably different from each other. This difference must be taken into account when analysing the data from closely spaced hot wires in the viscous sublayer.

From (6.1) the fluctuating velocity measured by a hot wire a distance y_1 from the wall is

$$u_1 - \bar{u}_1 = y_1(f - \bar{f}). \tag{6.3}$$

Similarly for a hot wire a distance y_2 from the wall (6.1) yields

$$u_2 - \bar{u}_2 = y_2(f - \bar{f}). \tag{6.4}$$

From (6.3) and (6.4) one obtains

$$\frac{u_1(t) - \bar{u}_1}{[(u_1(t) - \bar{u}_1)^2]^{\frac{1}{2}}} = \frac{f(t) - \bar{f}}{[(f(t) - \bar{f})^2]^{\frac{1}{2}}} = \frac{u_2(t) - \bar{u}_2}{[(u_2(t) - \bar{u}_2)^2]^{\frac{1}{2}}}. \tag{6.5}$$

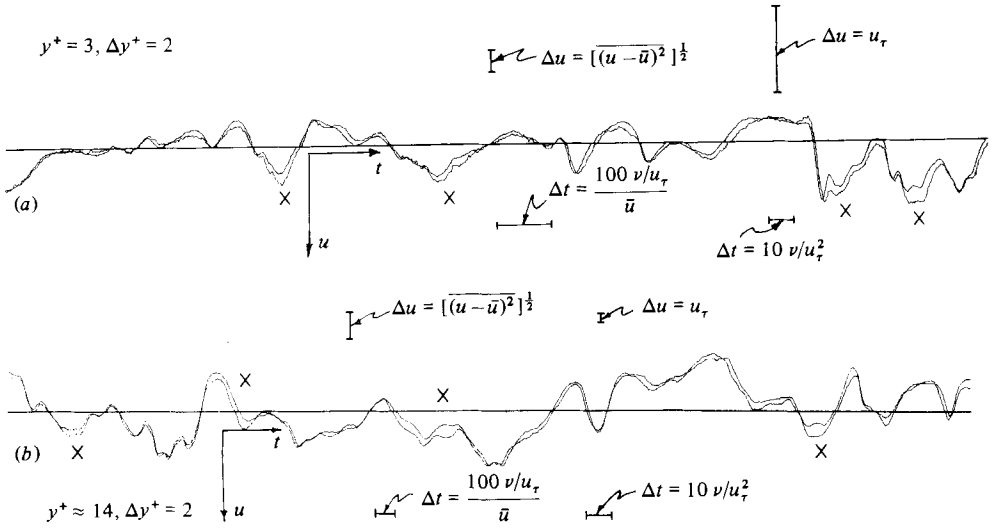

FIGURE 13. Computer plots of traces of the normalized velocity fluctuations from a pair of small hot wires at two points: (*a*) within the sublayer, $y^+ = 3$, $\Delta y^+ = 2$; (*b*) near point of maximum turbulent intensity, $y^+ = 14$, $\Delta y^+ = 2$. × marks location of intense small-scale shear layers.

From (6.5) it is apparent that when the streamwise velocity in the sublayer is described by (6.1), i.e. it is an unsteady linear function of the distance from the wall, the velocity fluctuations normalized by the root-mean-square velocity will be independent of y. Data from two probes in the sublayer can then be used to detect small-scale shear layers which cause a departure from the behaviour described by (6.1). It is only necessary to multiply the fluctuating signals from one of the hot wires by a constant value so that both have the same root-mean-square value. At any time that the two signals are not the same the difference between them indicates the presence of additional shear, of small scale, which causes a departure from the behaviour described by (6.1).

Also, consider two hot wires placed at a disturbance of 15 or more viscous lengths from the wall. The turbulent intensity in this region is approximately the same for hot wires with small spatial separation normal to the wall. The above procedure of normalizing the two fluctuating hot-wire signals so that they have the same root-mean-square velocity and then observing any differences between them can be used to detect the presence of small-scale shear layers in this region.

This normalization procedure was performed using a computer program which determined the mean and root-mean-square value of each hot-wire signal, for a time period of 16 s, and then multiplied the fluctuations about the mean for one hot wire by the ratio of the root-mean-square values. The two signals were then visually examined for the presence of small-scale shear layers. For example, when small-scale structure is not present one will have for hot wires 1 and 2

$$e_1(t) - \bar{e}_1 = (e_2(t) - \bar{e}_2)\,\frac{e_1'}{e_2'}, \tag{6.6}$$

where e_1' and e_2' are the root-mean-squares of the fluctuations about the mean of each hot-wire output voltage. When small-scale structure is present the above normalized voltages will not be equal. The magnitude of the inequality is a measure of the additional velocity gradient that occurs in a distance comparable to the spacing between the hot wires.

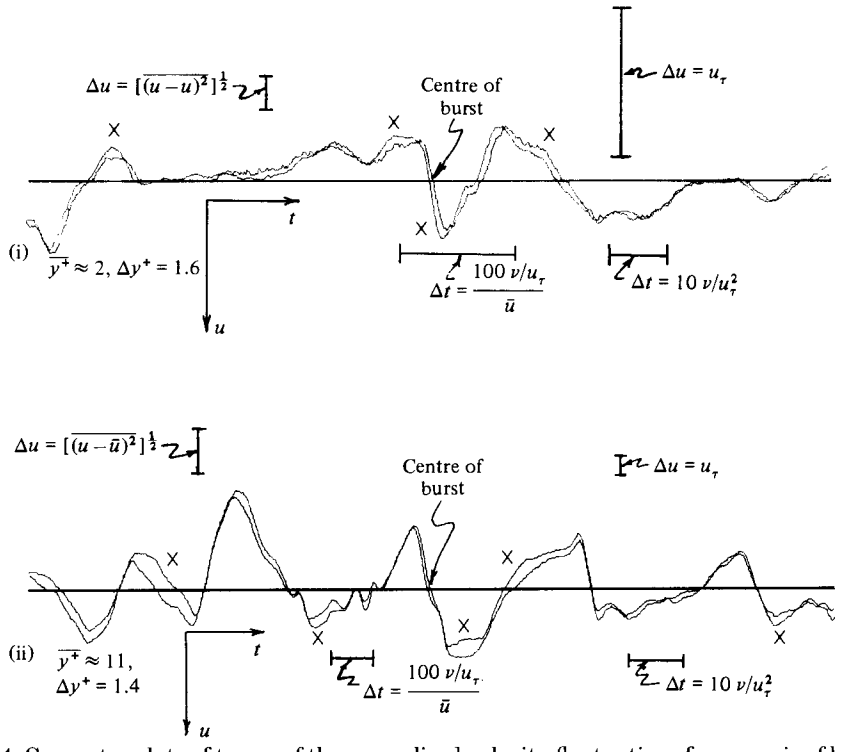

FIGURE 14. Computer plots of traces of the normalized velocity fluctuations from a pair of hot wires at two points when a burst was detected at the location of the upper wire: (i) within the sublayer, $y^+ = 3, \Delta y^+ = 2$; (ii) near point of maximum turbulent intensity, $y^+ = 14, \Delta y^+ = 2$. Burst detected at centre of plot. × marks location of intense small-scale shear layers.

Figure 13 is a typical computer plot of the normalized velocities that were measured by a pair of hot wires placed with the sublayer and well above the sublayer. The velocity and timescale for the traces is indicated on the figure. It is evident from figure 13 that occasionally intense small-scale shear layers were encountered by the two probes. Some examples are marked with a × on figure 13. The largest of the marked examples correspond to intermittent velocity gradients with a magnitude of the order of the mean shear at the wall.

6.2. *Analysis of the small-scale shear layers during a burst and when a burst does not occur*

To learn more about the intermittent small-scale shear layers in relation to the bursting phenomenon, the signals from the two hot wires, separated by a distance of two viscous lengths in a direction normal to the wall, were written onto a disc file when the VITA algorithm, described in §5.1, had found a burst at the position of the upper hot wire. Data for 85 viscous timescales ($t^+ = 85$) before and after the centre of each burst were written onto the disc file. Typically of the order of 100 bursts were encountered and stored for later analysis at a given location of the hot-wire pair.

Figure 14 is a plot of the normalized signals from a pair of hot wires placed within the sublayer (at an average value of $y^+ = 2.28$) and above the sublayer (at an average value of $y^+ = 11.16$) when a burst was detected by the upper hot wire. The detection time for the burst is at the centre of the plot. A small-scale shear layer of relatively long duration is evident just after the burst occurred on the pair of traces obtained at $y^+ = 2.28$, and there are two intense small-scale shear layers of short duration

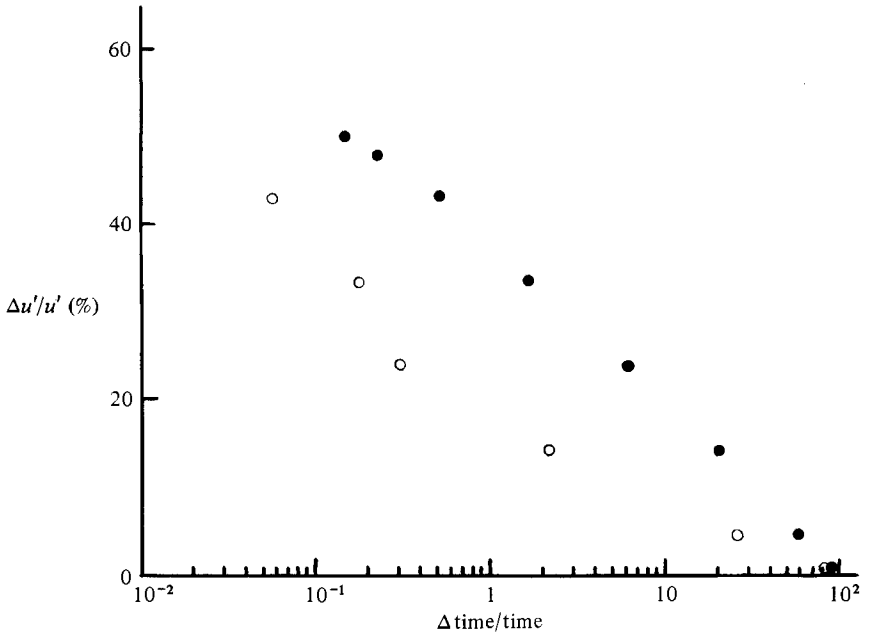

FIGURE 15. Fraction of the time that the difference in velocity measured by two hot wires is greater than a given fraction of the local root-mean-square velocity: ●, burst occurring; ○, not bursting. $Re_\ominus = 9840$, $y^+ = 2.28$, $\Delta y^+ = 1.61$.

evident on the pair of traces obtained at $y^+ = 11.16$. These events are indicated on figure 14. A visual examination was made of many similar computer traces during bursting. It appeared that the occurrence of intense small-scale shear layers was more frequent during bursting than at other times.

A computer program was developed to search for and perform a statistical analysis of the magnitude and frequency of occurrence of small-scale shear layers. The program calculated the percentage of the time that the difference beween the normalized signals from a pair of closely spaced hot wires was greater than a specified fraction of the root-mean-square velocity.

The program was used to search for small-scale shear layers during the time that a burst was detected. The VITA burst-detection algorithm used an averaging period of $10\nu/u_\tau^2$ with the burst-detection time at the centre. A time period T_S with $T_S u_\tau^2/\nu = 21$ and centred at the burst-detection time was used in the search for small-scale shear layers. The time T_S being longer than the burst detection time allowed the 'tails' of the burst signals to be included.

The program first normalized the velocity signal from each wire so that the short-time mean and the short-time root-mean-square velocities were the same during the period T_S. The absolute value of the difference between the normalized velocities of the two probes was determined and the percentage of the time period T_S that the absolute value of this difference was greater than a specified fraction of the long-time root-mean-square velocity was calculated. The results of the calculation are displayed in figures 15 and 16.

Also displayed in figures 15 and 16 are the results of the same calculation performed when no burst was occurring during the time period T_S at the same location. The data used when a burst did not occur were obtained at a time $t^+ = 170$ after a burst had

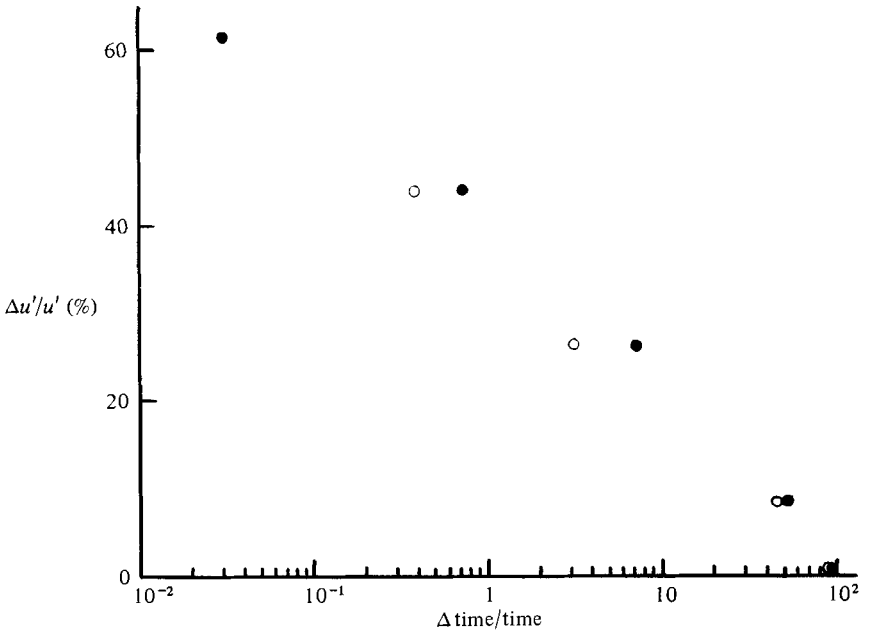

FIGURE 16. Fraction of the time that the difference in velocity measured by two hot wires is greater than a given fraction of the local root-mean-square velocity: ●, burst occurring; ○, not bursting. $Re_\theta = 9840$, $y^+ = 11.16$, $\Delta y^+ = 1.43$.

occurred. Note that the average time between bursts is of the order of $t^+ = 370$ (see figure 13), so that a burst is not likely at the time $t^+ = 170$ after a burst. However, a check was made to be sure that no bursts had occurred during the time $t^+ = 85$ before and after the above no-burst time.

The data displayed in figures 15 and 16 show that small-scale shear layers of a given magnitude occur more frequently during bursting than when bursts do not occur. In the viscous sublayer, at $y^+ = 2.28$, small-scale shear layers of a given magnitude occur during bursts approximately ten times more often than when bursts do not occur. Farther from the wall, at $y^+ = 11.16$, this difference is reduced to a factor of approximately two.

6.3. *Analysis of the small-scale shear layers shortly before and after a burst*

In addition to the above search for small-scale shear layers during a burst and when no burst occurred, a search for small-scale shear layers was made shortly before and after a burst had occurred. The length of the time period T_B during which a search was made for small-scale shear layers before and after a burst corresponds to $T_B u_\tau^2/\nu = 39$. The search was made for the time interval T_B centred at the time $t = 26\nu/u_\tau^2$ just before and just after each burst. The same computer program used in the previous analysis described in §6.2 was used for this analysis. The velocity signals were normalized in the same way, but for a time period of $T_B = 39\nu/u_\tau^2$.

The results of the search for small-scale shear layers before and after a burst had occurred are displayed in figures 17 and 18. From these results it is apparent that small-scale shear layers were found to occur more frequently shortly after a burst was detected than before the burst was detected. Also, there was a greater difference in the frequency of occurrence of small-scale shear layers of a given magnitude before

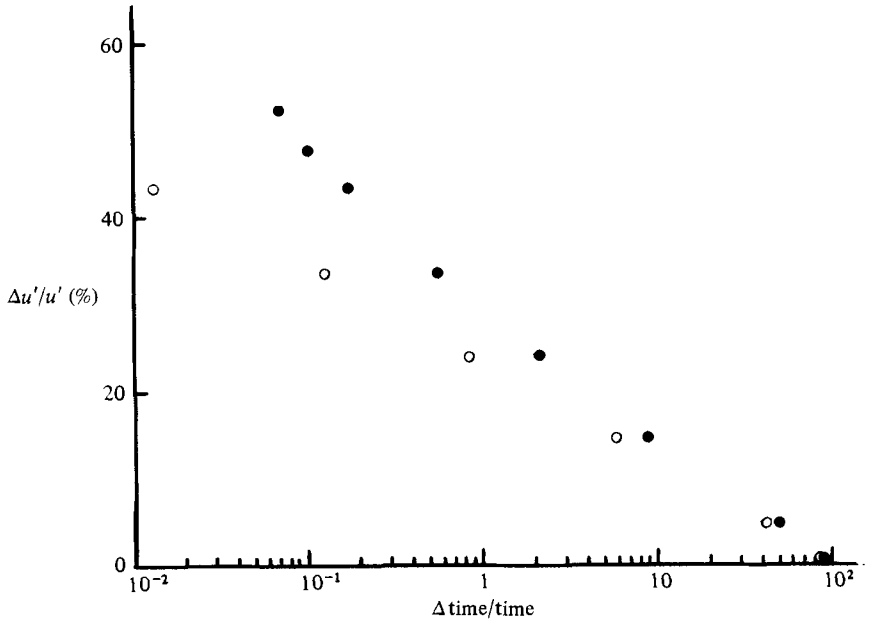

FIGURE 17. Fraction of the time that the difference in velocity measured by two hot wires is greater than a given fraction of the local root-mean-square velocity: ●, after a burst; ○, before a burst. $Re_\Theta = 9840$, $y^+ = 2.28$, $\Delta y^+ = 1.61$.

and after a burst at a distance of 2.2. viscous lengths from the wall than was found 11.2 viscous lengths from the wall.

6.4. *Other results from the analysis of small-scale shear layers*

Further analysis of the velocity data obtained with a pair of small hot wires was performed. The analysis is described in Sharma (1980). The major results of the analysis are described below.

The duration of the small-scale shear layers during the burst and non-bursting times was determined for the search time $T_S = 21\nu/u_\tau^2$. It was found that during a burst small-scale shear layers last for a longer period of time than during the time when bursts do not occur. It was also found that during a burst small-scale shear layers, at a distance of 11 viscous lengths from the wall, occur with a magnitude comparable to the mean shear at the wall 15 times more frequently with $\partial u/\partial y > 0$ than with $\partial u/\partial y < 0$.

The probability density distribution of the velocity from one wire and of the difference in the velocities sensed by a pair of hot wires was also determined at various distances from the wall. Nothing particularly surprising was found in this analysis. It was confirmed that during the burst time large-amplitude velocity fluctuations are more probable than at other times. This is, however, essentially the criterion on which the VITA burst-detection method is based. The probability density distribution of the difference in velocities from a pair of hot wires was also determined. It was concluded that the occurrence of small-scale shear layers is more probable during the bursting time than when a burst is not present, and the magnitude of the small-scale shear is greater during the bursting time than it is when a burst is not present.

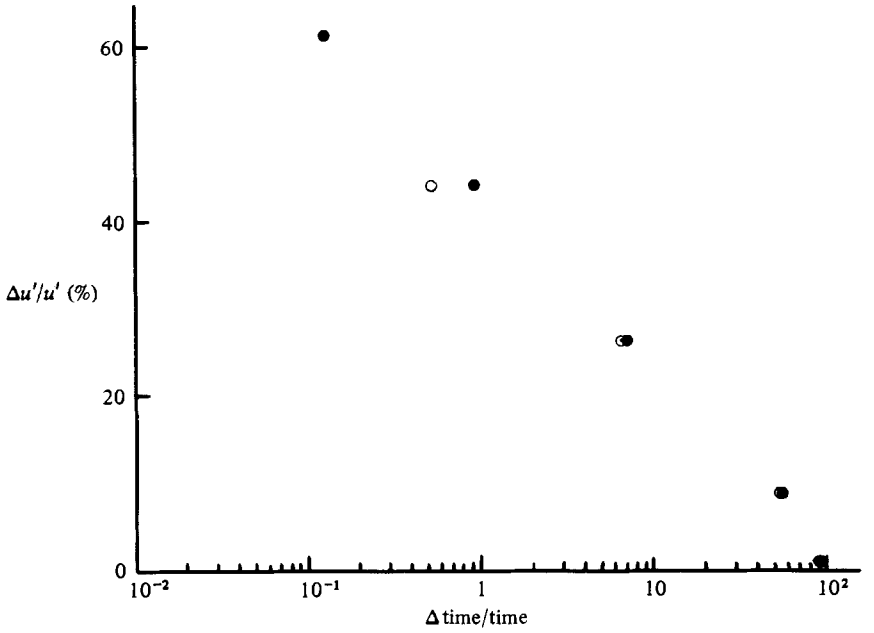

FIGURE 18. Fraction of the time that the difference in velocity measured by two hot wires is greater than a given fraction of the local root-mean-square velocity: ●, after a burst; ○, before a burst. $Re_\Theta = 9840$, $y^+ = 11.16$, $\Delta y^+ = 1.43$.

7. Summary and conclusions

The small hot wires that were fabricated and used in this investigation were difficult to make and to use for turbulence measurements. The hot wires were fragile and the voltage output often slowly changed with time. The cause of the slow drift of the output voltage was never definitely established, but it was probably caused by a combination of electromigration (Black 1969) and/or slow chemical reaction of residual amounts of the plating solution with the silver used to form the support prongs.

The end conditions for these low-aspect-ratio hot wires had a significant effect on their performance. The velocity sensitivity was low because the heat lost to the supporting prongs was large compared with the heat lost to the flow. For example, the temperature at the centre of a hot wire of aspect ratio 50 was more than twice the ambient temperature when the hot wire was heated to an average temperature 50% greater than the ambient temperature. Also, the aerodynamic interference of the supporting prongs is probably large. We did not study the aerodynamic interference, but the geometric configuration of the low-aspect-ratio hot wire suggests that it is significant. For example, the diameter of the silver plating used to form the supporting prongs was comparable to the length of the hot wire, and the most sensitive region, near the centre of the hot wire, was narrower than the diameter of the supporting prongs on either side.

The above problems were solved or avoided by *in situ* calibration of each hot wire for each measurement of the streamwise velocity component. Measurements of the streamwise component of turbulence in a boundary layer using hot wires of different lengths were made. Examination of measurements of the power spectrum of the

streamwise velocity fluctuations revealed that the power-spectral density at high frequencies was increased when the aspect ratio of the hot wires was reduced. The measurements showed that near the wall approximately 20 % of the turbulent energy could not have been resolved by conventionally sized hot wires.

Measurements of the streamwise velocity fluctuations were made with low-aspect-ratio hot wires, and the VITA burst-detection algorithm, devised by Blackwelder & Kaplun (1976), was used to determine the burst frequency. It was found that the burst frequency increased slowly as the distance of the hot wire from the wall was increased. At a distance of 15 viscous lengths from the wall the dimensionless burst frequency was found to be essentially constant and independent of Reynolds number when scaled with wall variables. The dimensionless burst frequency scaled with outer variables was found to increase when the Reynolds number was increased. These findings are in agreement with the recent results of Blackwelder & Haritonidis (1983).

Measurements of the streamwise velocity fluctuations were also made using two small hot wires placed in close proximity to each other. Simultaneous records of the velocity fluctuations from two probes separated by a distance of the order of two viscous lengths in a direction normal to the wall were studied and analysed to determine the magnitude and statistical properties of small-scale shear layers. It was found that small-scale fluctuations in the velocity gradient $\partial u/\partial y$ as large as the mean shear at the wall were intermittently present in the turbulent flow near the wall. A digital computer algorithm was used to perform a simple statistical analysis of the frequency of occurrence of these small-scale shear layers. It was found that small-scale shear layers occurred most frequently when bursts were present in the flow near the wall. Small-scale shear layers occur less frequently after a burst and even less frequently just before a burst occurs. It was also determined that during a burst, at a distance of 11 viscous lengths from the wall, small-scale shear layers occur with a magnitude comparable to the mean shear at the wall 15 times more frequently with positive $\partial u/\partial y$ than with negative $\partial u/\partial y$. From these results it is apparent that, at relatively high Reynlolds numbers, the bursting process produces turbulence in the flow near the wall which contains shear-layer fluctuations whose scale is of the order of the viscous length.

The research was sponsored by the National Science Foundation under Grant ENG76-80214. The suggestions of the referees and helpful discussions with Timothy Wei, who read and commented on the revised manuscript, are gratefully acknowledged.

REFERENCES

Betchov, R. 1952 Nonlinear theory of a hot-wire anemometer. *NACA Tech. Memo.* 1346.

Black, J. R. 1969 Electromigration – a brief survey and some recent results. *IEEE Trans. on Electron Devices*, ED **16**, 338.

Blackwelder, R. F. & Haritonidis, J. H. 1983 The bursting frequency in turbulent boundary layers. *J. Fluid Mech.* **132**, 87.

Blackwelder, R. F. & Kaplan, R. E. 1976 On the wall structure of the turbulent boundary layer. *J. Fluid Mech.* **76**, 89.

Bull, M. & Thomas, A. S. W. 1976 High frequency wall-pressure fluctuations in turbulent boundary layers. *Phys. Fluids* **19**, 597.

Chen, C. P. & Blackwelder, R. F. 1978 The large-scale motion in a turbulent boundary layer: a study using temperature contamination. *J. Fluid Mech.* **89**, 1.

COLES, D. E. 1955 The law of the wall in turbulent shear flow. In *50 Jahre Grenzschichtforschung*, p. 153. Vieweg.

COLLIS, D. C. & WILLIAMS, M. J. 1959 Two-dimensional convection from heated wires. *J. Fluid Mech.* **6**, 357.

CORINO, E. R. & BRODKEY, R. S. 1969 A visual investigation of the wall region in turbulent flow. *J. Fluid Mech.* **37**, 1.

ECKELMANN, H. 1974 The structure of the viscous sublayer and the adjacent wall region in a turbulent channel flow. *J. Fluid Mech.* **65**, 439.

EMMERLING, R. 1973 The instantaneous structure of the wall pressure under a turbulent boundary layer flow. *Max-Planck-Inst. Stromungsforsch. Rep.* 9/1973.

FAGE, F. A. & TOWNEND, H. C. H. 1932 An examination of turbulent flow with an ultramicroscope. *Proc. R. Soc. Lond.* A **135**, 656.

GUPTA, A. K., LAUFER, J. & KAPLAN, R. E. 1971 Spatial structure in the viscous sublayer. *J. Fluid Mech.* **50**, 493.

HAMA, F. R., LONG, J. D. & HEGARTY, J. C. 1957 On transition from laminar to turbulent flow. *J. Appl. Phys.* **28**, 388.

HUMMEL, R. E. & BREITLING, R. M. 1971 On the direction of electromigration in thin silver, gold, and copper films. *App. Phys. Lett.* **18**, 373.

KASTRINAKIS, E. G. 1977 *Max-Planck-Inst. Strömungsforsch. Rep.* 5/1977.

KIM, H. T., KLINE, S. J. & REYNOLDS, W. C. 1971 The production of turbulence near a smooth wall in a turbulent boundary layer. *J. Fluid Mech.* **50**, 133.

KLEBANOFF, P. S. 1954 Characteristics of turbulence in a boundary layer with zero pressure gradient. *NACA Tech. Note* 3178.

KLINE, S. J., REYNOLDS, W. C., SCHRAUB, F. A. & RUNSTADLER, P. W. 1967 The structure of turbulent boundary layers. *J. Fluid Mech.* **30**, 741.

KOVASZNAY, L. S. G., KIBENS, V. & BLACKWELDER, R. F. 1970 Large scale motion in the intermittent region of a turbulent boundary layer. *J. Fluid Mech.* **41**, 305.

KRONAUER, R. E. 1953 Survey of hot-wire theory and techniques, *Div. Appl. Sci., Harvard Univ.* (*Pratt & Whitney Res.*) *Rep.* 137.

KREPLIN, H. P. & ECKELMANN, H. 1979 Propagation of perturbations in the viscous sublayer and adjacent wall region. *J. Fluid Mech.* **95**, 305.

LAUFER, J. & BADRI NARAYANAN, M. A. 1971 Mean period of the turbulent production mechanism in a turbulent boundary layer. *Phys. Fluids* **14**, 182.

LU, S. S. & WILLMARTH, W. W. 1972 Measurements of the structure of the Reynolds stress in a turbulent boundary layer. *J. Fluid Mech.* **60**, 481.

NARAHARI RAO, K., NARASIMHA, R. & BADRI NARAYANAN, M. A. 1971 The bursting phenomena in a turbulent boundary layer. *J. Fluid Mech.* **48**, 339.

SHARMA, L. 1980 Study of turbulent structure with hot-wires smaller than the viscous length. Ph.D. thesis, University of Michigan.

WILLMARTH, W. W. & BOGAR, T. J. 1977 Survey and new measurements of turbulent structure near the wall. *Phys. Fluids Suppl.* **20**, S9.

WILLMARTH, W. W., WINKEL, R. E., SHARMA, L. K. & BOGAR, T. J. 1976 Axially symmetric turbulent boundary layers on cylinders. *J. Fluid Mech.* **76**, 35.

WILLS, J. A. B. 1962 The correction of hot-wire readings for proximity to a solid boundary. *J. Fluid Mech.* **12**, 388.